A High Frequency Coupled Inductor Design for High Power Density DC-DC Converters

Ahmed H. Ismail, Zhuxuan Ma, Ahmad Al-Hmoud, and Yue Zhao
Power Electronic Systems Laboratory at Arkansas (PESLA)
Department of Electrical Engineering, University of Arkansas
Fayetteville, AR, 72701, USA
Email: {ahismail, zm009, aalhmoud, yuezhao}@uark.edu

***Abstract*—Coupled inductors has been extensively adopted in DC-DC converters due to their distinctive features, such as the flux cancelation ability, enhanced performance, higher power density and lower weight compared to their non-coupled counterparts. The fast-switching speed of the wide bandgap power electronics demands high frequency, high density, and more efficient passive components, especially the inductors. In this paper, we present a high frequency coupled inductor design using parallel air gaps and copper foil windings with the commercial off-the-shelf planar magnetic cores. The proposed inductor is prototyped and demonstrated in a four-phase interleaved, 50 kW boost converter. The developed inductor prototype has a volume less than 0.5 L and a resonant frequency over 7 MHz with much lower ac resistance compared to a printed circuit board (PCB) based inductor.**

Keywords—Coupled inductor, dc-dc converter, high frequency, planar inductor

I. Introduction

Coupled inductors can improve the performance and the dynamic response of non-isolated DC-DC converters [1]-[2]. Converters using coupled inductors can have higher power density and reduced weight compared to their counterparts using non-coupled inductors. Another benefit of the coupled inductor is the flux cancelation in the core, which reduces the core losses and hence a smaller core can be used. Recently, with the advancement of wide bandgap devices, such as the SiC and GaN power devices, switching frequency of power electronic converters have significantly increased, raising with it the demand for high frequency, high density, and highly efficient inductors.

For a high frequency inductor, two important factors must be carefully considered: the resonant frequency and the ac resistance. Planar cores are popular in high density applications due to their low profile and enhanced thermal distribution. However, traditionally they incorporated with printed circuit board (PCB) windings, which offer high reproducibility at the expense of high cost, especially when the number of turns increase. In addition, there is a low degree of flexibility in controlling the winding parameters, e.g., the turn-turn parasitic capacitance, due to the limitations in the PCB stack customization.

To decrease the ac resistance, several solutions have been reported, e.g., using parallel and orthogonal air gaps [3], which however may require custom magnetic cores. [4] suggested the use of vertically oriented copper foil which also offers several advantages such as reduced cost, control over inductor parameters and high reproducibility. Based on these concepts, a coupled inductor design is presented in this paper. A 3D printed bobbin is used to control the geometry of a copper foil winding, inserted vertically around the outer legs of the core, hence leading to a parallel air gap which in turn leads to the lower ac resistance. Moreover, because the turn to turn spacing can be accurately controlled so is the parasitic capacitance and eventually the resonant frequency. The result is a high frequency, low ac resistance coupled inductor set. A case study of a four-phase interleaved boost converter is adopted as a design example. A prototype of the inductor is built and tested on the converter and results are presented in this paper.

II. High Frequency Coupled Inductor Design

A. Coupled Inductors in DC-DC Converters

Fig. 1 shows the schematic of a typical multiphase boost or buck converter, a four-phase example is shown. For multiphase converters with more than two phases, the inductors should be distributed among the phases so as to maintain a 180° phase shift between the currents in a coupled inductor pair. This is to maximize the flux cancelation in a single core, to reduce the core losses and increase the saturation point.

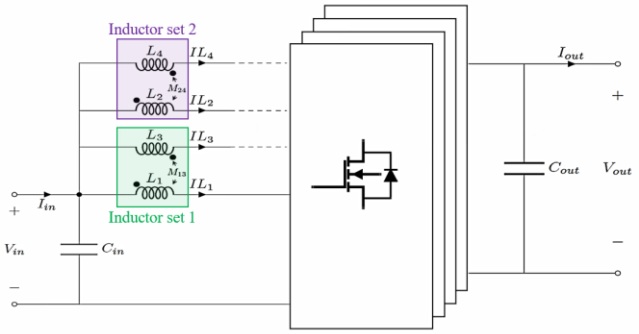

Fig. 1. Schematic of a multiphase DC-DC converter with inverse coupled inductor (4-phase example)

This work was supported in part by the U.S. National Science Foundation (NSF) under CAREER Award ECCS-1751506 and also in part by the NSF Engineering Research Center for Power Optimization of Electro Thermal Systems (POETS) with cooperative agreement EEC-1449548.

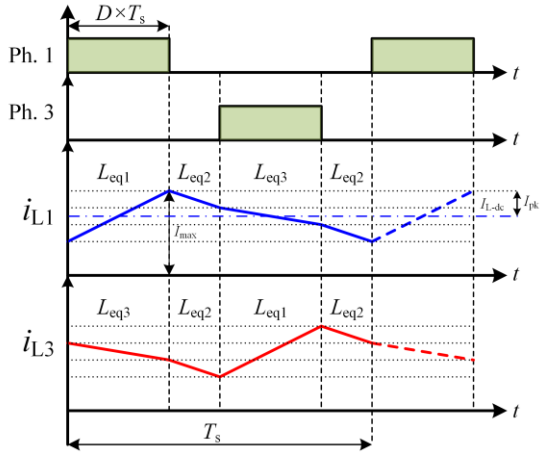

Fig. 2. Inductor current waveforms with inversely coupled inductor for D < 0.5

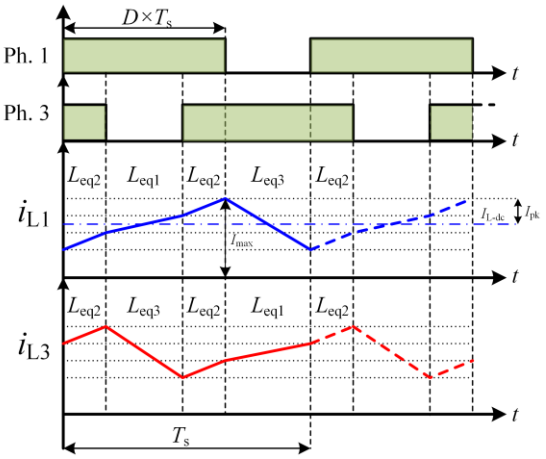

Fig. 3. Inductor current waveforms with inversely coupled inductor for D > 0.5

As shown in Figs. 2 and 3, the coupling effect changes the voltages across each inductor in the coupled inductor pair due to the mutual flux which causes the current slopes to change in four distinct periods. This leads to different equivalent inductances in each of these time periods, i.e., L_{eq1}, L_{eq2} and L_{eq3}. L_{eq1} and L_{eq3} set the peak inductor current when $D < 0.5$ and $D > 0.5$ respectively, consequently they directly impact the inductor ripple current.

From [1], L_{eq1} or L_{eq3} can be written as:

$$L_{eq1}\left(\text{or } L_{eq3}\right) = \alpha \times L \tag{1}$$

where α is a function of the coupling coefficient k and the duty cycle D and is given by:

$$\begin{cases} \alpha = \frac{1-k^2}{1+k\frac{D}{D'}} & D < 0.5 \\ \alpha = \frac{1-k^2}{1+k\frac{D'}{D}} & D > 0.5 \end{cases} \tag{2}$$

If k is negative, i.e., inverse coupling, then α can be greater than 1 depending on the operating point D, which means that L_{eq1} (or L_{eq3}) is greater than the self-inductance L. The coupling factor k is a constant once the inductor is designed, hence it should be selected at the design stage to achieve the required performance across the operating duty cycle range.

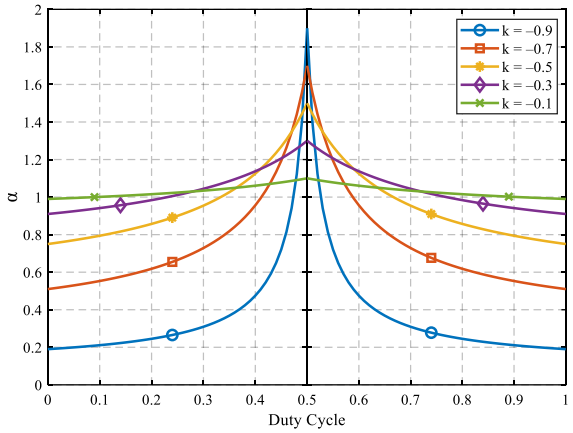

Fig. 4. Plot of α as a function of duty cycle for different k values

According to Fig. 4, which shows α versus the duty ratio according to (2), depending on the operating duty cycle range, a coupling coefficient k can be selected to achieve $\alpha > 1$ in this range. As a result, for the same self-inductance value, the inductor ripple current can be reduced according to:

$$\Delta i_L = \frac{V_{in}\left(1-\frac{V_{in}}{V_{out}}\right)}{2\alpha \times L \times f_{sw}} \tag{3}$$

Conversely, if the ripple current is to be maintained, this could translate to a smaller inductance value with smaller inductor size. Then the reduced inductance value can be calculated from:

$$L \geq \frac{V_{in}\left(1-\frac{V_{in}}{V_{out}}\right)}{2\alpha \times \Delta i_L \times f_{sw}} \tag{4}$$

Nevertheless, an α greater than 1 is desirable. Since the duty cycle depends on the operating point, therefore, a coupling coefficient value k, that will keep $\alpha>1$ for the converter's operating range, is chosen. However, not every k value can be easily achieved since it depends on the physical magnetic core geometry. Therefore, the objective in selecting k is to choose one that achieves $\alpha>1$ in a wide operation range and at the same time can be realized without using complicated magnetic core geometries.

In contrast to the steady state operation, where a large inductance value is preferred, large inductance values slow down the dynamic response of the converter. However, for the inverse coupled inductor L_{eq2} is responsible for the dynamic response of the converter [1], where $L_{eq2} = (1+k)\,L$, and since k is negative, L_{eq2} is always smaller than L. Therefore, the converter can have faster dynamic response than that with uncoupled inductors.

B. Coupled Inductor Design

Fig. 5 shows the coupled inductor core structure used in this work with its equivalent magnetic circuit. It consists of two E cores separated by an air gap of length l_g. Two coils with equal number of turns N are wound, in the same direction, on the outer legs of the construction. There are several methods to select the optimal core size such as the area product method. However, for

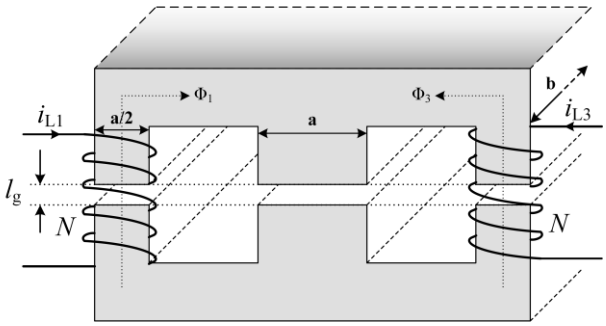

Fig. 5. Coupled inductor core structure

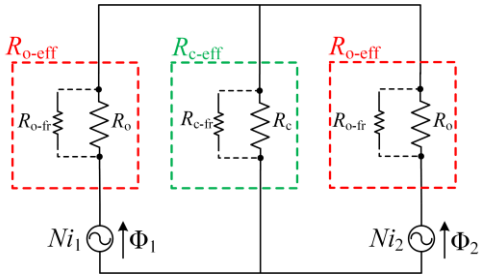

Fig. 6. Magnetic circuit

high power density designs, planar ferrite core is selected due to their low profile and improved thermal performance. Unlike other core shapes, there are not so many off-the-shelf choices for planar ferrite core, therefore, the largest off-the-shelf *E* core was selected which is the E64/50/10 [5].

A proper material should be selected according to the frequency and saturation flux. For the inductor described here 3F36 material from Ferroxcube is selected for the core, which is suitable for high frequency operation with low losses. In addition, it has high saturation flux. 3C92 can be an alternative. To ensure enough safety margin and account for the high temperature operation, the maximum flux was set to 350 mT in this design.

From the magnetic circuit in Fig. 6, the ideal inductances and coupling coefficient k can be derived as:

$$\begin{cases} L = \frac{N^2\times(R_o+R_c)}{R_o(R_o+2R_c)} \\ M = -\frac{N^2\times R_c}{R_o(R_o+2R_c)} \\ k = \frac{M}{L} = -\frac{R_c}{R_o+R_c} \end{cases} \quad (5)$$

Choosing an equal air gap in the outer and center legs will yield $k = -0.33$ by substituting $R_o = 2R_c$ in (5) which will simplify the core structure from one hand and keep $\alpha > 1$ for a wide converter operation region as seen from Fig. 4.

The minimum number of turns, required to keep the flux from exceeding a maximum desired design value B_{max}, corresponding to a maximum inductor current I_{max}, in the outer leg of the core, is calculated from:

$$N_{min} = \left\lceil \frac{(L+M)I_{max}}{B_{max}\times A_o} \right\rceil \quad (6)$$

where, $A_o = (a/2) \times b$ is the cross-sectional area of the outer leg. Then the ideal air gap length not considering the fringing effect can be calculated from:

$$l_{g-ideal} = \frac{3N_{min}^2\times\mu_o\times A_o}{4L} \quad (7)$$

The fringing effect caused by the air gap can increase the effective cross-sectional area of the air gap, thus reducing the reluctance causing the actual inductance value to increase and the core may saturate early due to the increased flux density. Therefore, the air gap length should be adjusted to account for the fringing effect and keep the core from saturation. One simple method to account for the fringing effect is to treat the fringing effect as a parallel reluctance as described in [6] as shown in Fig. 6. Equations (8) and (9) can be used to identify the actual air gap l_g.

$$\begin{cases} A_{c-eff} = (a + 2l_g) \times (b + 2l_g) \\ A_{o-eff} = (0.5a + 2l_g) \times (b + 2l_g) \end{cases} \quad (8)$$

$$\begin{cases} R_{c-eff} = R_c \parallel R_{c-fr} = \frac{l_g}{\mu_o\times A_{c-eff}} \\ R_{o-eff} = R_o \parallel R_{o-fr} = \frac{l_g}{\mu_o\times A_{o-eff}} \end{cases} \quad (9)$$

The inductance values can be recalculated from (5) using the effective reluctances from (9). Finally, the maximum flux density can be rechecked using the recalculated inductances to ensure it does not exceed the maximum value:

$$B = \frac{(L+M)I_{max}}{N\times A_{o-eff}} < B_{max} \quad (10)$$

Based on the design process discussed in this section, the key parameters of the inductor are given in Table I.

TABLE I: INDUCTOR KEY PARAMETERS

Parameter	Value
L	50 µH
f_{sw}	150 kHz
I_{max}	40 A
k	−1/3
Core	EE64/50/10 – 3F36
a	10.2 mm
b	50.8 mm
B_{max}	350 mT
N	15
l_g	2 mm

C. HF Coupled Inductor Concept

Parallel and orthogonal air gaps have been shown to have several advantages over the conventional perpendicular air gap [3]. They help mitigate the fringing effect on the windings and hence improve the ac resistance. However, to realize the parallel air gap, ferrite machining by grinding is required which can be difficult and could possibly lead to increased core loss. In the proposed design, by changing the orientation of the winding [4], the air gap has become parallel to the winding without having to customize the core.

In the conventional air gap core design with PCB winding, the magnetic field around the air gap can cause the current to concentrate in the middle of the winding. This affects all the

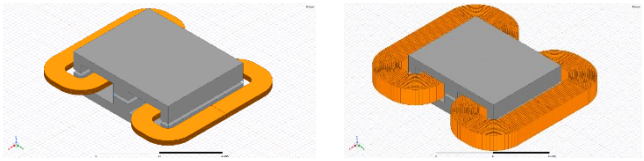

(a) (b)

Fig. 7. ANSYS simulation for (a) conventional PCB winding and (b) vertical winding with parallel air gap

turns in case of PCB winding since they are all in parallel. However, in case of the vertical winding configuration, the magnetic field affects the closer winding because the field strength decays over distance. As a result, the vertical winding is expected to have lower ac resistance. This is verified through ANSYS simulations as shown in Figs. 7(a) and (b). Both simulated inductor sets have the same parameters except for winding/air gap orientation. Fig. 8 shows a reduction in the ac resistance of more than 50% in case of the vertical winding compared to a horizontal one at 150 kHz.

Fig. 9 shows the inductor key parameters that affect the overall dc and ac resistances of the winding. Copper foil thickness W_{cu} is one of the key design parameters. The requirements for W_{cu} conflict between ac and dc resistances. Obviously, increasing the copper width decreases the dc resistance (for the same winding length), but it increases the ac resistance due to the skin effect. To reduce the ac resistance, the copper width W_{cu} should be selected less than the skin depth δ at the desired frequency f, sometimes as low as $\delta/3$. The skin depth of copper can be calculated from:

$$\delta\ (\mathrm{m}) = \sqrt{\frac{1.678\times10^{-8}\ (\Omega.\mathrm{m})}{\pi f \times \left(4\pi\times10^{-7}\ (\frac{\mathrm{H}}{\mathrm{m}})\right)\times 0.999}} \quad (11)$$

The total winding loss can be calculated from:

$$P_{loss-cu} = P_{\mathrm{dc}} + P_{\mathrm{ac}} = I^2_{\mathrm{L-dc}} \times R_{\mathrm{dc}} + I^2_{\mathrm{L-rms}} \times R_{\mathrm{ac}} \quad (12)$$

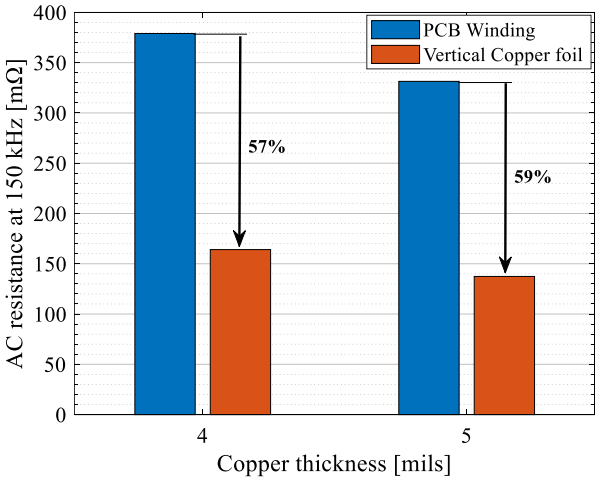

Fig. 8. AC resistance comparison between PCB winding and vertical copper foil

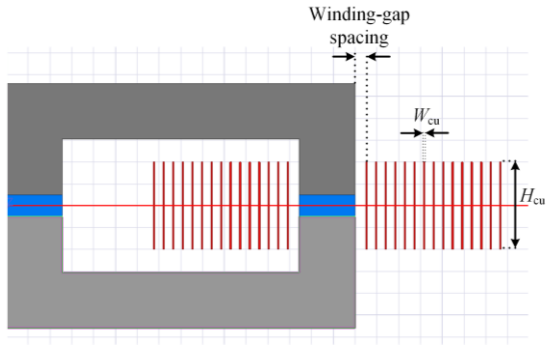

Fig. 9. Inductor key parameters

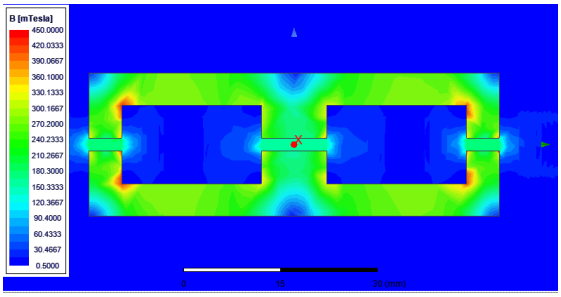

Fig. 10. ANSYS flux density distribution of the coupled inductor set at full load.

where $I_{\text{L-rms}} \approx I_{\text{pk}} / \sqrt{3}$, since the inductor current is close to a triangular shape. The ac resistance is a result of the skin and proximity effects as well as fringing flux effect. Therefore, an optimization is required to find the global minimum winding loss. For instance, if the converter is operating in continuous conduction mode and the ac ripple current is very low, this means that the dc is the dominant loss, consequently, minimizing R_{dc} should be favored and vice versa.

Copper foil height H_{cu} is another important design parameter. After selecting the optimal W_{cu} value, copper height is one degree of freedom to reduce the dc resistance without hurting the ac resistance. Therefore, H_{cu} should be maximized in the available winding window.

The spacing between the air gaps and the winding is another important factor to consider in the bobbin design. The farther the winding is from the air gap the lower ac resistance it has due to the weakening of the magnetic field as distance increases. Winding shaping approach has been proposed in [7]-[8]. However, placing the winding far from the air gap means that its overall length will increase, hence, increasing the dc resistance. Therefore, again, a tradeoff needs to be addressed.

An insight into the effect of different parameters on the ac resistance is shown in Table II. It suggests that the further the winding is located from the air gap, the lower the ac resistance will be, which is expected as discussed earlier. Fig. 10 shows the flux density distribution in the core at full load and confirms that it is below the target maximum design value.

TABLE II: EFFECT OF DESIGN PARAMETERS ON THE AC RESISTANCE

W_{Cu}	H_{Cu}	Winding-Gap Spacing	R_{ac} @150 kHz
3 mils	10 mm	3 mm	260 mΩ
4 mils	10 mm	3 mm	213 mΩ
4 mils	10 mm	4 mm	164 mΩ
5 mils	10 mm	4 mm	137 mΩ
5 mils	10 mm	5 mm	128 mΩ

III. INDUCTOR PROTOTYPING

Fig. 11 shows the coupled inductor configuration. Each inductor pair are coupled on a single core, but no coupling exists between the two pairs. This is to simplify the inductor and converter design. However, a common bobbin is used to fit all inductors to make the tolerance between them tight. Vertical windings of uninsulated copper foil are shaped and inserted into spiral slots in a 3D printed bobbin. Planar ferrite *E* cores are inserted in an open slot in the bobbin and an equal air gap, made from 3D printed shims, is inserted on the outer and center legs.

Fig. 12 shows a cross section of the bobbin. The bobbin prototype is fabricated by 3D printing using the ABS material which has dielectric strength of approximately 12 kV/mm. The winding turns are separated by 500 µm separator that serves as an insulator. This thickness can be optimized, within the limits of manufacturing capability, to achieve simultaneous targets, e.g., insulation, inductor size and minimizing parasitic capacitance. This leads to greater control over the inductor's critical parameters, a flexibility which is lacking in PCB based windings due to the limitations in PCB stack customization.

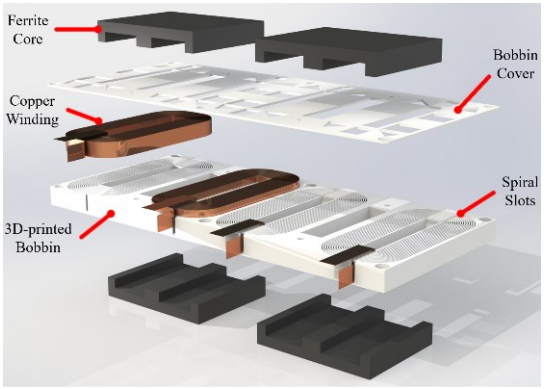

Fig. 11. Exploded 3D rendering of the proposed coupled inductor

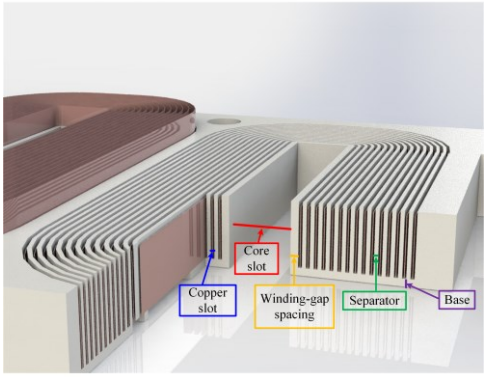

Fig. 12. Bobbin cross section with key parameters labeled

IV. EXPERIMENTAL RESULTS

Fig. 13 shows the first fabricated prototype of the inductors sets. The overall dimensions are 200mm×90mm×22mm, which is approximately 0.4 L in volume. In this first prototype iteration, the copper height was 8.5 mm, the copper width was 4 mils and the winding-gap spacing was 2 mm. Figs. 14 and 15 are the measured inductance and resistance respectively which are close to the simulated values given in Table II. Measurements were carried out using the Keysight 4990A impedance analyzer. It is clear from Fig. 14 that the resonance frequency is more than 7 MHz. The dc and ac resistances are 87 mΩ and 246 mΩ at 150 kHz respectively. The inductor prototype is used in a four-phase DC-DC boost converter with parameters shown in Table. III. Fig. 16 shows the currents of one coupled inductor pair, i.e., i_{L1} and i_{L3}, and the inductor voltage at a 40 kW output power, while Fig. 17 shows the waveforms of the multiphase boost converter at 40 kW output power.

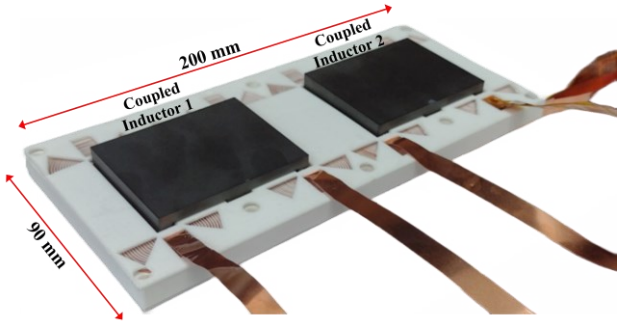

Fig. 13. Coupled inductor prototype

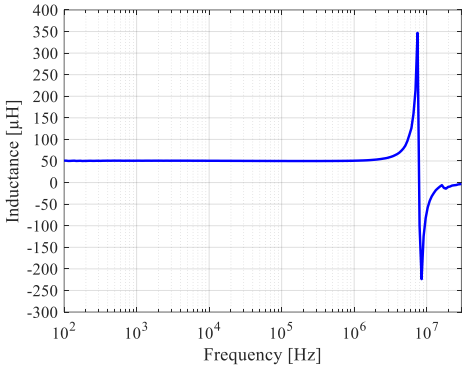

Fig. 14. Inductance measurement

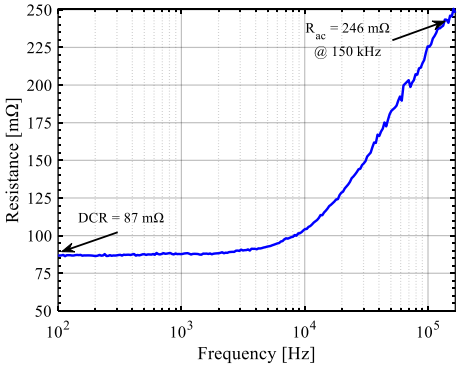

Fig. 15. Inductor series resistance measurement

TABLE III. BOOST CONVERTER KEY PARAMETERS

Parameter	Symbol	Value
Power	P_{out}	50 kW
Output Voltage	V_{out}	800 V
Input Voltage	V_{in}	350–500 V
Max. Input Current	$I_{in.max}$	100 A
Number of Phases	n	4
Switching Frequency	f_{sw}	150 kHz
Inductor Current Ripple	Δi_L	50%
Inductance	L	50 µH
Inductor Coupling factor	k	-0.33

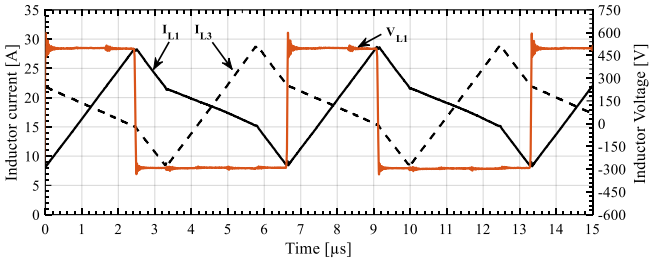

Fig. 16. Inductor waveforms during a 40 kW converter test

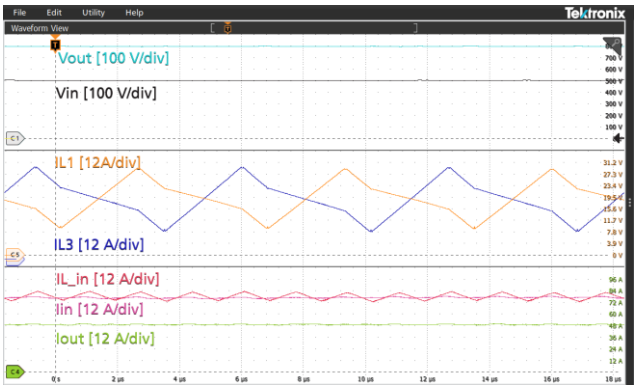

Fig. 17. Multiphase boost converter test at 40 kW, 800 V output

V. CONCLUSION

In this paper, a coupled inductor design based on perpendicular air gap and copper foil is presented. Instead of customizing the core to insert a parallel air gap, the coil is wound vertically using copper foil around the outer legs of an off-the-shelf EE core set. This reduced the ac resistance and increased the resonance frequency compared to a PCB inductor. Moreover, the 3D printed bobbin gives great flexibility over the winding geometry, hence the critical parameters can be controlled. Additionally, for high number of turns, this is much quicker and more cost-effective solution than PCB based windings. The effects of some critical design parameters on the inductor performance are presented here and a first iteration prototype is shown and is tested on a 50 kW DC-DC converter. A future optimized iteration will be fabricated, which offers lower DC and AC resistance preserving the same inductor size as the first prototype, this will be achieved through optimizing the design parameters.

REFERENCES

[1] P.-L. Wong, P. Xu, P. Yang and F. C. Lee, “Performance improvements of interleaving VRMs with coupling inductors,” in IEEE Transactions on Power Electronics, vol. 16, no. 4, pp. 499-507, July 2001, doi: 10.1109/63.931059.

[2] M. Pavlovský, G. Guidi and A. Kawamura, “Assessment of Coupled and Independent Phase Designs of Interleaved Multiphase Buck/Boost DC–DC Converter for EV Power Train,” in IEEE Transactions on Power Electronics, vol. 29, no. 6, pp. 2693-2704, June 2014, doi: 10.1109/TPEL.2013.2273976.

[3] S. Mukherjee, Y. Gao and D. Maksimović, “Reduction of AC Winding Losses Due to Fringing-Field Effects in High-Frequency Inductors With Orthogonal Air Gaps,” in IEEE Transactions on Power Electronics, vol. 36, no. 1, pp. 815-828, Jan. 2021, doi: 10.1109/TPEL.2020.3002507.

[4] A. H. Wienhausen, A. Sewergin, S. P. Engel and R. W. De Doncker, “Highly efficient power inductors for high-frequency wide-bandgap power converters,” 2017 IEEE 12th International Conference on Power Electronics and Drive Systems (PEDS), 2017, pp. 442-447, doi: 10.1109/PEDS.2017.8289111.

[5] Ferroxcube, E64/10/50 + PLT64/50/5 datasheet, 2016, Accessed: Nov. 15, 2022. [online]. Available: https://www.ferroxcube.com/upload/media/product/file/Pr_ds/E64_10_50_PLT64_50_5.pdf

[6] Z. Yang, H. Suryanarayana and F. Wang, "An Improved Design Method for Gapped Inductors Considering Fringing Effect," 2019 IEEE Applied Power Electronics Conference and Exposition (APEC), 2019, pp. 1250-1256, doi: 10.1109/APEC.2019.8721811.

[7] J. D. Pollock and C. R. Sullivan, "Loss models for shaped foil windings on low-permeability cores," 2008 IEEE Power Electronics Specialists Conference, 2008, pp. 3122-3128, doi: 10.1109/PESC.2008.4592432.

[8] N. Simpson and P. H. Mellor, "Additive manufacturing of shaped profile windings for minimal AC loss in gapped inductors," 2017 IEEE International Electric Machines and Drives Conference (IEMDC), 2017, pp. 1-7, doi: 10.1109/IEMDC.2017.8002337.